Title
Thin THz QCL active regions for improved continuous-wave operating temperature

Journal
AIP Advances, 11(12)

ISSN
2158-3226

Authors
Curwen, Christopher A
Addamane, Sadhvikas J
Reno, John L
et al.

Publication Date
2021-12-01

DOI
10.1063/5.0071953

Thin THz QCL active regions for improved continuous-wave operating temperature

Christopher A. Curwen,[1,a)] Sadhvikas J. Addamane,[2] John L. Reno,[2] Mohammad Shahili,[3] Jonathan H. Kawamura,[1] Ryan M. Briggs,[1] Boris S. Karasik[1], and Benjamin S. Williams[3]

[1]*Jet Propulsion Laboratory, California Institute of Technology, Pasadena, CA 91109, USA.*
[2]*Sandia National Laboratories, Center of Integrated Nanotechnologies, MS 1303, Albuquerque, New Mexico 87185, USA*
[3]*Department of Electrical and Computer Engineering, University of California, Los Angeles, California 90095, USA*

[a)]*Author to whom correspondence should be addressed: chris.a.curwen@jpl.nasa.gov*

We compare the performance of 10 μm and 5 μm thick metal-metal waveguide terahertz quantum-cascade laser ridges operating around 2.7 THz and based on a 4-well phonon depopulation active region design. Thanks to reduced heat dissipation and lower thermal resistance, the 5 μm thick material shows an 18 K increase in continuous wave operating temperature compared to the 10 μm material, despite a lower maximum pulsed-mode operating temperature and a larger input power density. A maximum continuous wave operating temperature of 129 K is demonstrated using the 5 μm thick material and a 15 μm wide ridge waveguide that lased up to 155 K in pulsed mode. The use of thin active regions is likely to become increasingly important to address the increasing input power density of emerging 2- and 3-well active region designs that show the highest pulsed operating temperatures.

THE MANUSCRIPT

THz quantum-cascade lasers (QCLs) are compact, efficient semiconductor sources of coherent radiation in the 1 - 6 THz range [1, 2], but they require cryogenic cooling, which limits the actual size and power of a usable laser to that of the cryocooler. In the laboratory environment this is an inconvenience, but in certain applications, such as space-based astrophysical heterodyne receivers, it is unacceptable. To date, the maximum operating temperature of a THz QCL in continuous-wave (cw) is 129 K [3]. Higher temperatures can be achieved by operating devices in a low duty-cycle pulsed mode (e.g. 1 μs bias pulses repeated at 10 kHz), but this makes many applications difficult, if not impossible (heterodyne local oscillators, dual frequency comb spectroscopy, etc.). The pursuit of maximum pulsed operating temperature has garnered significant attention in the field, and the best report now stands at 250 K using a thermoelectric cooler [4]; however the strategies for obtaining maximum pulsed and maximum cw temperature do not necessarily align. Part of the trend to achieve higher pulsed operation has been to reduce the number of quantum-wells in a single period of the active gain material, and increase the barrier heights to reduce leakage into higher energy states and the continuum [4-14]. Shorter period designs lend themselves to higher gain thanks to more transitions per volume (larger average doping for the same sheet doping), and faster depopulation of the of the lower laser level

(enabled by direct optical phonon scattering) [4, 11, 14]. Additionally, they tend to show less temperature-induced leakage current (and a higher characteristic temperature T_0), which may be due to more diagonal radiative transitions with longer upper state lifetimes, and/or a reduced state space for temperature-induced non-radiative scattering out of the upper laser level. However, these short period designs tend to require larger applied electric fields and draw larger current densities. This increased input power dissipation density works against high temperature cw operation due to increased heating. This trade-off must be optimized to achieve the highest cw operating temperature. So far, the thermal benefit of low-bias, long-period designs has outweighed the higher pulsed operating temperatures of high-bias, short-period designs, as the current record cw temperature performance was achieved with a low-bias 9-well active region design [3].

Aside from active region design, improving cw operating temperature can be approached via waveguide design. Metal-metal waveguides have been used for the majority of high temperature cw THz QCL demonstrations thanks to (a) the strong mode confinement which maximizes modal gain and minimizes losses, and (b) the transverse waveguide dimensions can be scaled below far below the wavelength, which reduces total power consumption [15]. Epitaxy-side down mounting to sapphire and AlN substrates allows heat extraction from both the top and bottom sides of laser ridges, and has demonstrated improved cw operation for surface plasmon THz QCLs, as well as mid-IR QCLs [16, 17]. Buried heterostructures are a key technology that has improved cw operating temperatures for narrow mid-IR QCL ridges via improved heat removal from the sidewalls [18-20]. While the use of buried heterostructures has also somewhat improved the cw operation of THz QCLs, the strategy has not been widely adopted as it requires an inconvenient ion implantation step [21, 22].

One simple route to reduce heating during cw operation is to use thinner QCL gain material, which is the primary thermal bottleneck due to its large out-of-plane thermal conductivity ($\kappa_\perp$) around 5-10 W/(m·K) [23-25]. This is close to an order of magnitude lower than bulk GaAs material due to the reduced phonon velocities and increased phonon scattering that takes place within the GaAs/$Al_xGa_{1-x}As$ heterostructures. In Figure 1, the simulated temperature difference ΔT between the heat sink and the average temperature in the QCL (approximately the temperature in the middle of the device) is plotted as a function of input power density and device thickness, assuming a thermal conductance of 7.5 W/(m·K). A number of data points on high-temperature devices from existing literature are

indicated by the dashed vertical green (3-well) and red (2-well) lines. Reducing the thickness by a factor of two should reduce ΔT by a factor of 3 to 4.

While the thermal benefits of a reduced active region are clear, it must be considered that reducing the thickness of the active region also increases the threshold gain of the laser. The waveguide design becomes critical in this case. With surface-plasmon (SP) waveguides, the confinement of the THz mode to the gain material decreases as the active region is made thinner, and previous studies indicate it is unlikely the that the thermal advantage will outweigh the increase in threshold for cw operation [26]. On the other hand, metal-metal (MM) waveguides provide nearly unity mode confinement even as the thickness decreases. Though the waveguide loss coefficient related to the metallic cladding increases inversely with active region thickness, it is only one component of the total loss, and experimental pulsed-mode data indicates much less penalty in reducing the active region thickness of a MM waveguide compared to SP waveguides [27, 28]. The strong mode confinement of MM waveguides results in low outcoupling efficiency and poor beam quality from typical facet emitting devices, and thinner waveguides make these problems worse. However, large area MM surface-emitting [29, 30] and end-fire arrays [31] can provide much better power and beam quality, and such arrays should benefit from thin active regions, which allow for larger area arrays for a given total input power. Cw lasing was demonstrated with a 6 μm thick MM waveguide and a 9-well active region design in Ref. [32], but the maximum cw temperature was only 60 K, and no direct comparisons were made to thicker active regions.

In this Letter we demonstrate that the thermal benefit of reducing the active region thickness from 10 μm to 5 μm in a MM waveguide can outweigh the increase in threshold gain, which results in a net increase in cw operating temperature. The active region is a 4-well phonon-depopulation design used for this study is similar to that in [33], but modified to operate around 2.7 THz. The specific layer sequence for a single module (in Å, GaAs/**$Al_{0.15}Ga_{0.45}As$**) is 106/**20**/106/**37**/88/**40**/<u>172</u>/**51**. The middle 88 Å of the underlined well is Si-doped at 5×10^{16} cm^{-3}. Two wafers were grown, one with 162 modules for a total of 10 μm of material, and one with 80 modules for a total of 5 μm of material. The 10 μm thick wafer was grown at Sandia National Laboratory (wafer number VA1034), while the 5 μm thick wafer was grown by a commercial vendor, IQE plc. The growths were capped with a 50 nm n^{++} GaAs layer (5×10^{18} cm^{-3}) and a 35 nm low-temperature grown GaAs layer to enable an Ohmic contact. The wafers were processed via Cu-Cu thermocompression wafer bonding into 50 μm × 1 mm metal-metal waveguides with dry etched facets. Waveguiding was obtained by a Ta/Cu (15/600 nm) bottom cladding/contact layer, and a Ti/Au (15/250 nm) top cladding/contact

layer. Capacitance vs. voltage measurements estimate average doping levels of 6.4×10^{15} cm^{-3} (10% lower than design) and 7.8×10^{15} cm^{-3} (10% higher than design) for the 10 μm and 5 μm thick material, respectively.

Pulsed and cw data from the two wafers are presented in Figure 2. First, we note that the subthreshold leakage current and the maximum current density J_{max} is larger in the 5 μm wafer. This is likely due to the different doping densities in the two growths. Interestingly, in pulsed mode, the maximum operating temperature for the 5 μm thick material (T_{max}=156 K) was only 5 K lower than that of the 10 μm material (T_{max}=161 K). This is much smaller than the 20 K difference observed in [27], and is likely explained by the higher J_{max} in our 5 μm material, which may result in increased gain that compensates for the increased waveguide loss (larger population inversion).

The threshold current density is plotted as a function of the heat-sink temperature in the insets of Fig. 2, and the characteristic temperatures, T_0, as determined by fitting the data to the expression $J_{th} = J_0 \exp(T/T_0)$, is 112 K and 102 K for the 10 μm and 5 μm thick material, respectively. In cw, T_0 is 55 K and 65 K for the 10 μm and 5 μm thick material, respectively. The 5 μm shows reduced degradation in characteristic temperature when operating in cw, which demonstrates the advantages of the improved heat sinking. Absolute power data was not collected as the high temperature, small device size, and poor outcoupling and collection efficiency from a metal-metal facet result in low power levels, close to the noise level of our calibrated power meters.

In cw, the 5 μm thick material lases up to 118 K, while the 10 μm material only lases to 100 K. Not only is the maximum operating temperature of the 5 μm material higher, but the difference between the maximum pulsed and cw operating temperatures is smaller for the 5 μm material than the 10 μm material, despite the fact that the input power density is >50% larger for the 5 μm material than the 10 μm material (12.8×10^{12} W/m^3 versus 8.0×10^{12} W/m^3, respectively). Based on the experimentally observed difference between pulsed and cw temperatures, by fitting to simulation data we can estimate $\kappa_\perp$ of the 5 μm and 10 μm thick wafers to be 4.5 and 6.5 W/(m·K), respectively (effective thermal resistance values of 12.4 K/W and 14.9 K/W respectively). This estimate is made using a basic 2-D FEM model of an infinitely long ridge, assuming no thermal resistance at the metal ground plane of the QCL or the substrate contact to the heat sink. Ideally the voltage on the 5 μm device would be half that of the 10 μm device, but in experiment, the voltage was only reduced by the ~60% due to the existence of a Schottky contact voltage drop that is not affected by device thickness. We also note, it is possible that the 10 μm thick material would show a higher pulsed temperature if the doping was increased to that of the 5 μm material. Simulations indicate that, with the current

density the increased to 900 A/cm^2 (assuming $\kappa_\perp$ = 6.5 W/(m·K) and 11.5 V bias), the 10 μm thick material would have to lase up to 200 K in pulsed mode just to match the 129 K cw operating temperature of the 5 μm material. This is possible, but seems unlikely as it would imply a 45 K difference in pulsed temperature between a 10 μm and 5 μm ridge, which is much larger than previously observed. Based on the results in [27] and this study, it seems unlikely that the reduced waveguide loss of a 10 μm waveguide would increase the pulsed operating temperature by such a large margin.

To further push the cw limit, we fabricated 15 μm wide MM ridges using the 5 μm thick material, which according to simulation ($\kappa_\perp$ = 6.5 W/(m·K)), should reduce ΔT from 38 K to 31 K. Indeed, we achieve (Fig. 3) a maximum pulsed operating temperature of 155 K, identical to the 50 μm wide ridge, but we achieve a maximum cw operating temperature of 129 K, 11 K higher than the 50 μm wide device. This is exactly tied with the current cw temperature record achieved with a 10 μm thick, 9-well design in [3].

In conclusion, we have demonstrated the advantages of thinner MM waveguides for optimization the cw operating temperature of THz QCLs. By using a 4-well phonon depopulation design, a 5 μm thick active region device was demonstrated up to 129 K at 2.7 THz. We propose that the value of this approach will be even greater for the new generation of active region designs with T_{pulsed} >200 K. These designs exhibit very large power dissipation densities, and due to the larger Al fraction in the barriers may have even worse thermal conductivity. Considering the 2- and 3-well designs in Fig. 1, and the effects of thinner waveguides reported in [27, 28], it is possible that some of these devices might already be able to operate at cw temperatures in the 140 - 150 K range if thinner active regions were used. Together with strategies to reduce power dissipation density in the direct phonon depopulation scheme (e.g. the split-well design of [13]), this provides a path to cw operation of THz QC-lasers at temperatures reachable by thermoelectric coolers (~200 K).

ACKNOWLEDGMENTS

This research was carried out in part at the Jet Propulsion Laboratory, California Institute of Technology, under a contract with the National Aeronautics and Space Administration. 5 μm wafer material was grown by IQE plc. Microfabrication was performed at the UCLA Nanofabrication Laboratory. This work was performed, in part, at the Center for Integrated Nanotechnologies, an Office of Science User Facility operated for the U.S. Department of Energy (DOE) Office of Science. Sandia National Laboratories is a multimission laboratory managed and operated

by National Technology and Engineering Solution of Sandia, LLC, a wholly owned subsidiary of Honeywell International, Inc., for the U.S. Department of Energy's National Nuclear Security Administration under Contract No. DE-NA0003525. Partial funding was provided by the National Aeronautics and Space Administration (No. 80NSSC19K0900).

AUTHOR DECLARATIONS

The authors have no conflicts to disclose

DATA AVAILABILITY STATEMENT

The data that supports the findings of this study are available within the article.

REFERENCES

[1] R. Kohler, A. Tredicucci, F. Beltram, H. E. Beere, E. H. Linfield, A. G. Davies, D. A. Ritchie, R. C. Iotti, and F. Rossi, "Terahertz semiconductor-heterostructure laser," Nature **vol**. 417, 156-159 (2002).

[2] B. S. Williams, "Terahertz quantum-cascade lasers," Nat Photonics **vol**. 1, 517-525 (2007).

[3] M. Wienold, B. Roben, L. Schrottke, R. Sharma, A. Tahraoui, K. Biermann, and H. T. Grahn, "High-temperature, continuous-wave operation of terahertz quantum-cascade lasers with metal-metal waveguides and third-order distributed feedback," Opt Express **vol**. 22, 3334-3348 (2014).

[4] A. Khalatpour, A. K. Paulsen, C. Deimert, Z. R. Wasilewski, and Q. Hu, "High-power portable terahertz laser systems," Nat Photonics (2020).

[5] M. A. Belkin, J. A. Fan, S. Hormoz, F. Capasso, S. P. Khanna, M. Lachab, A. G. Davies, and E. H. Linfield, "Terahertz quantum cascade lasers with copper metal-metal waveguides operating up to 178 K," Opt Express **vol**. 16, 3242-3248 (2008).

[6] S. Kumar, Q. Hu, and J. L. Reno, "186 K operation of terahertz quantum-cascade lasers based on a diagonal design," Appl Phys Lett **vol**. 94, (2009).

[7] S. Fathololoumi, E. Dupont, C. W. I. Chan, Z. R. Wasilewski, S. R. Laframboise, D. Ban, A. Matyas, C. Jirauschek, Q. Hu, and H. C. Liu, "Terahertz quantum cascade lasers operating up to similar to 200 K with optimized oscillator strength and improved injection tunneling," Opt Express **vol**. 20, 3866-3876 (2012).

[8] C. W. I. Chan, Q. Hu, and J. L. Reno, "Tall-barrier terahertz quantum cascade lasers," Appl Phys Lett **vol**. 103, (2013).

[9] A. T. Jiang, A. Matyas, K. Vijayraghavan, C. Jirauschek, Z. R. Wasilewski, and M. A. Belkin, "Experimental investigation of terahertz quantum cascade laser with variable barrier heights," J Appl Phys **vol**. 115, (2014).

[10] A. Albo, Q. Hu, and J. L. Reno, "Room temperature negative differential resistance in terahertz quantum cascade laser structures," Appl Phys Lett **vol**. 109, (2016).

[11] M. Franckie, L. Bosco, M. Beck, C. Bonzon, E. Mavrona, G. Scalari, A. Wacker, and J. Faist, "Two-well quantum cascade laser optimization by non-equilibrium Green's function modelling," Appl Phys Lett **vol**. 112, (2018).

[12] M. A. Kainz, S. Schonhuber, A. M. Andrews, H. Detz, B. Limbacher, G. Strasser, and K. Unterrainer, "Barrier Height Tuning of Terahertz Quantum Cascade Lasers for High-Temperature Operation," Acs Photonics **vol**. 5, 4687-4693 (2018).

[13] A. Albo, Y. V. Flores, Q. Hu, and J. L. Reno, "Split-well direct-phonon terahertz quantum cascade lasers," Appl Phys Lett **vol**. 114, (2019).

[14] L. Bosco, M. Franckie, G. Scalari, M. Beck, A. Wacker, and J. Faist, "Thermoelectrically cooled THz quantum cascade laser operating up to 210K," Appl Phys Lett **vol**. 115, (2019).

[15] B. S. Williams, S. Kumar, Q. Hu, and J. L. Reno, "Operation of terahertz quantum-cascade lasers at 164 K in pulsed mode and at 117 K in continuous-wave mode," Opt Express **vol**. 13, 3331-3339 (2005).

[16] O. Kruger, S. Kreutzmann, D. Prasai, M. Wienold, R. Sharma, W. Pittroff, L. Weixelbaum, W. John, K. Biermann, L. Schrottke, F. Schnieder, G. Erbert, H. T. Grahn, and G. Trankle, "Epitaxial-Side Mounting of Terahertz Quantum-Cascade Lasers for Improved Heat Management," Ieee Photonic Tech L **vol**. 25, 1570-1573 (2013).

[17] Y. Y. Li, J. Q. Liu, F. Q. Liu, J. C. Zhang, S. Q. Zhai, N. Zhuo, L. J. Wang, S. M. Liu, and Z. G. Wang, "High power-efficiency terahertz quantum cascade laser," Chinese Phys B **vol**. 25, (2016).

[18] Q. Y. Lu, S. Slivken, D. H. Wu, and M. Razeghi, "High power continuous wave operation of single mode quantum cascade lasers up to 5 W spanning lambda similar to 3.8-8.3 µm," Opt Express **vol**. 28, 15181-15188 (2020).

[19] A. Lyakh, R. Maulini, A. Tsekoun, R. Go, and C. K. N. Patel, "Tapered 4.7 µm quantum cascade lasers with highly strained active region composition delivering over 4.5 watts of continuous wave optical power," Opt Express **vol**. 20, 4382-4388 (2012).

[20] W. J. Zhou, Q. Y. Lu, D. H. Wu, S. Slivken, and M. Razeghi, "High-power, continuous-wave, phase-locked quantum cascade laser arrays emitting at 8 µm," Opt Express **vol**. 27, 15776-15785 (2019).

[21] S. Dhillon, J. Alton, S. Barbieri, C. Sirtori, A. de Rossi, M. Calligaro, H. E. Beere, and D. Ritchie, "Ultralow threshold current terahertz quantum cascade lasers based on double-metal buried strip waveguides," Appl Phys Lett **vol**. 87, (2005).

[22] J. Alton, S. S. Dhillon, C. Sirtori, A. de Rossi, M. Calligaro, S. Barbieri, H. E. Beere, E. H. Linfield, and D. A. Ritchie, "Buried waveguides in terahertz quantum cascade lasers based on two-dimensional surface plasmon modes," Appl Phys Lett **vol**. 86, (2005).

[23] G. Scamarcio, M. S. Vitiello, V. Spagnolo, S. Kumar, B. Williams, and Q. Hu, "Nanoscale heat transfer in quantum cascade lasers," Physica E **vol**. 40, 1780-1784 (2008).

[24] S. Fathololoumi, E. Dupont, D. Ban, M. Graf, S. R. Laframboise, Z. R. Wasilewski, and H. C. Liu, "Time-Resolved Thermal Quenching of THz Quantum Cascade Lasers," Ieee J Quantum Elect **vol**. 46, 396-404 (2010).

[25] M. A. Kainz, M. Wenclawiak, S. Schonhuber, M. Jaidl, B. Limbacher, A. M. Andrews, H. Detz, G. Strasser, and K. Unterrainer, "Thermal-Dynamics Optimization of Terahertz Quantum Cascade Lasers with Different Barrier Compositions," Phys Rev Appl **vol**. 14, (2020).

[26] M. Salih, P. Dean, A. Valavanis, S. P. Khanna, L. H. Li, J. E. Cunningham, A. G. Davies, and E. H. Linfield, "Terahertz quantum cascade lasers with thin resonant-phonon depopulation active regions and surface-plasmon waveguides," J Appl Phys **vol**. 113, (2013).

[27] E. Strupiechonski, D. Grassani, D. Fowler, F. H. Julien, S. P. Khanna, L. Li, E. H. Linfield, A. G. Davies, A. B. Krysa, and R. Colombelli, "Vertical subwavelength mode confinement in terahertz and mid-infrared quantum cascade lasers," Appl Phys Lett **vol**. 98, (2011).

[28] S. Kumar and Q. Hu, "Investigation of possible microcavity effect on lasing threshold of nonradiative-scattering-dominated semiconductor lasers," Appl Phys Lett **vol**. 100, (2012).

[29] T. Y. Kao, Q. Hu, and J. L. Reno, "Phase-locked arrays of surface-emitting terahertz quantum-cascade lasers," Appl Phys Lett **vol**. 96, (2010).

[30] L. Y. Xu, C. A. Curwen, P. W. C. Hon, Q. S. Chen, T. Itoh, and B. S. Williams, "Metasurface external cavity laser," Appl Phys Lett **vol**. 107, (2015).

[31] A. Khalatpour, J. L. Reno, and Q. Hu, "Phase-locked photonic wire lasers by pi coupling," Nat Photonics **vol**. 13, 47-+ (2019).

[32] Y. Chassagneux, J. Palomo, R. Colombelli, S. Barbieri, C. Sirtori, C. Sirtori, H. Beere, J. Alton, and D. Ritchie, "Low threshold THz QC lasers with thin core regions," Electron Lett **vol**. 43, 285-286 (2007).

[33] M. I. Amanti, G. Scalari, R. Terazzi, M. Fischer, M. Beck, J. Faist, A. Rudra, P. Gallo, and E. Kapon, "Bound-to-continuum terahertz quantum cascade laser with a single-quantum-well phonon extraction/injection stage," New J Phys **vol**. 11, (2009).

Figure Captions

Fig. 1. Overview of THz QCL thermal dissipation problem. (*left*) Simulated temperature difference (ΔT) between the average temperature within the QCL active region and heat sink as a function of active region input power density and three different device thicknesses (10 μm, 5 μm, and 2.5 μm, solid black lines). The input power density and $T_{max,pulsed}$ for a number of samples from the literature are indicated by the dashed vertical lines and the blue shaded region [4, 6, 7, 9, 12-14]. The expected $T_{max,cw}$ for each design can be inferred by subtracting the simulated ΔT for a given active region thickness. It should be noted that the $T_{max,pulsed}$ values from the literature were reported for 10 μm thick devices and will be impacted by reduced active region thickness. (*right*) Thermal simulation setup (not to scale).

Fig. 2. Pulsed (top) and cw (bottom) *L-I-V* data for the a) 10 μm thick and b) 5 μm thick devices. *I-V*'s are taken at 78 K. Threshold current versus heat-sink temperature and the fitted characteristic temperatures (T_0) are plotted in the insets of the figures.

Fig. 3. Cw *L-I-V* data for a 5 μm thick, 15 μm wide, 2.7 mm long MM ridge waveguide at 78 K. Inset shows lasing spectrum.

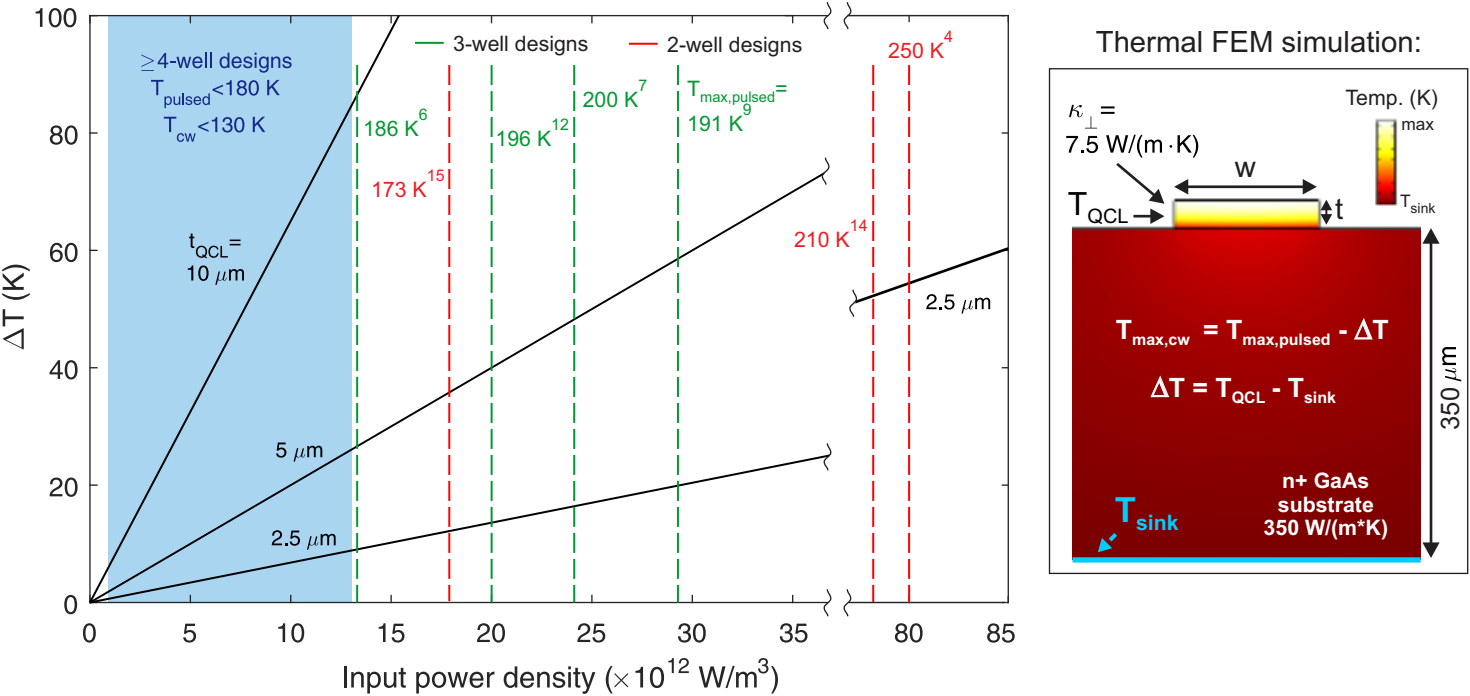
≥4-well designs
T_pulsed<180 K
T_cw<130 K
3-well designs
2-well designs
186 K^6
173 K^15
196 K^12
200 K^7
T_max,pulsed=
191 K^9
250 K^4
210 K^14
t_QCL=
10 μm
5 μm
2.5 μm
2.5 μm
ΔT (K)
Input power density (×10^12 W/m^3)
Thermal FEM simulation:
κ⊥ =
7.5 W/(m·K)
Temp. (K)
max
T_sink
w
T_QCL
t
T_max,cw = T_max,pulsed - ΔT
ΔT = T_QCL - T_sink
350 μm
n+ GaAs
substrate
350 W/(m*K)
T_sink

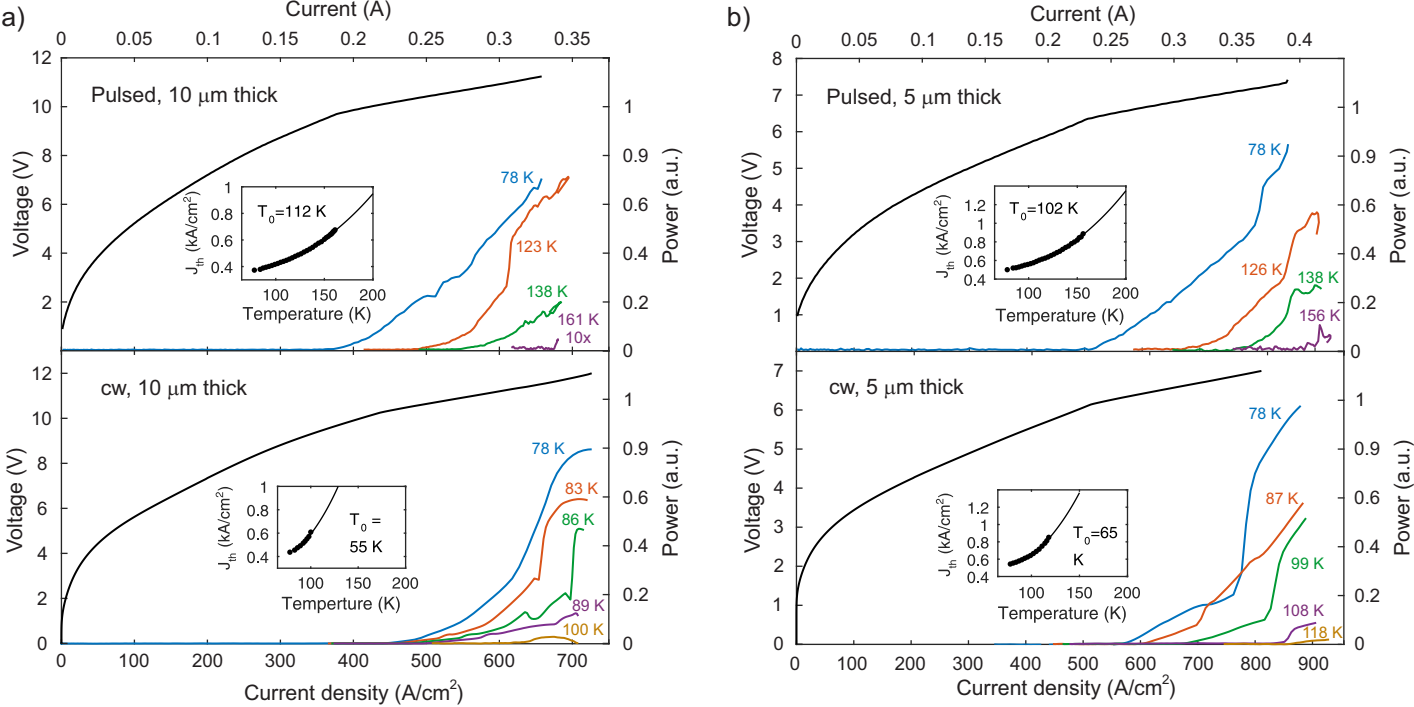
a)
Current (A)
Pulsed, 10 μm thick
Voltage (V)
Power (a.u.)
78 K
123 K
138 K
161 K
10x
T0=112 K
Jth (kA/cm2)
Temperature (K)
cw, 10 μm thick
78 K
83 K
86 K
89 K
100 K
T0 = 55 K
Temperture (K)
Current density (A/cm2)
b)
Current (A)
Pulsed, 5 μm thick
78 K
126 K
138 K
156 K
T0=102 K
cw, 5 μm thick
78 K
87 K
99 K
108 K
118 K
T0=65 K
Current density (A/cm2)

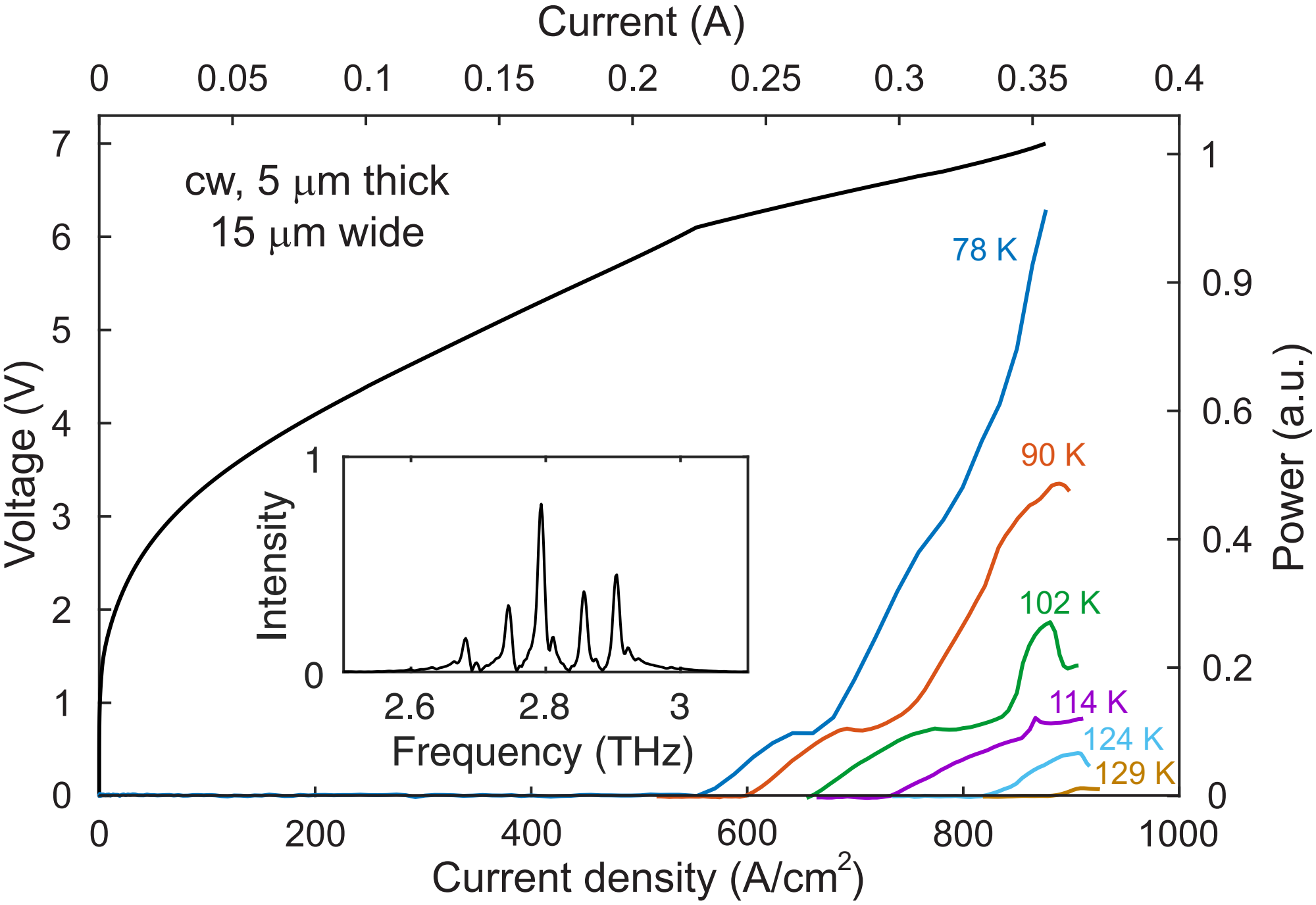
Current (A)
0
0.05
0.1
0.15
0.2
0.25
0.3
0.35
0.4
cw, 5 μm thick
15 μm wide
78 K
90 K
102 K
114 K
124 K
129 K
Voltage (V)
Power (a.u.)
Current density (A/cm²)
0
200
400
600
800
1000
Intensity
Frequency (THz)
2.6
2.8
3